Journal of Materials Chemistry C

Investigation of Ferrimagnetism and Ferroelectricity in $Al_xFe_{2-x}O_3$ Thin Films

Journal:	*Journal of Materials Chemistry C*
Manuscript ID	TC-ART-10-2019-005390.R1
Article Type:	Paper
Date Submitted by the Author:	14-Nov-2019

Complete List of Authors:	Rao, Badari Narayana; Tokyo Institute of Technology - Suzukakedai Campus, Laboratory for Materials & Structures Yasui, Shintaro; Tokyo Institute of Technology, Laboratory for Materials and Structures Katayama, Tsukasa; The University of Tokyo, Department of Chemistry Taguchi, Ayako; Japan Fine Ceramics Center, Nanostructures Research Laboratory Moriwake, Hiroki; Japan Fine Ceramics Center, Nanostructures Research Laboratory Hamasaki, Yosuke; National Defense of Academy Itoh, Mitsuru; Tokyo Institute of Technology, Materials and Structures Laboratory

ARTICLE

Investigation of Ferrimagnetism and Ferroelectricity in $Al_xFe_{2-x}O_3$ Thin Films

Received 1st October 2019,

Badari Narayana Rao,*[a] Shintaro Yasui,[a] Tsukasa Katayama,[b] Ayako Taguchi,[c,d] Hiroki Moriwake,[c,d] Yosuke Hamasaki[e] and Mitsuru Itoh[a]

$Al_xFe_{2-x}O_3$ (x-AFO) thin films, belonging to the κ-Al_2O_3 family are interesting because they show room temperature ferrimagnetism and have a polar crystal structure. These class of materials are being studied to observe simultaneous ferrimagnetism and ferroelectricity, and possibility of coupling between the two. However, it is difficult to realise their ferroelectric properties at room temperature, due to low resistivity of the films. In this work, we have optimized the synthesis conditions to obtain x-AFO ($0.5 \leq x \leq 1$) thin films with high resistance. While magnetic measurements confirmed room temperature ferrimagnetism of the films, the maximum magnetization was observed for the composition $x = 0.8$. In addition, the Curie temperature was found to be influenced by oxygen pressure during deposition. Ferroelectric measurements on the films showed small remnant polarization (~ 0.5 – 2 $\mu C/cm^2$). In contrast, the predicted polarization from first principles calculations was calculated to be between 21 - 26 $\mu C/cm^2$. The analysis also suggested that ferroelectric domain switching occurs through shearing of in-plane oxygen layers. Presence of multiple in-plane domains which oppose polarization switching of adjacent domains, is suggested to be the cause for the small observed polarization. The magnetocapacitance measurements showed weak magnetic coupling with the capacitance.

Introduction

Single-phase multiferroic materials have attracted considerable attention among scientists, due to strong drive in the industry towards device miniaturization and prospect of new functionalities in the field of sensors, memories, and spintronics.[1–6] However, most of the known multiferroic materials have very low operational temperatures, thereby limiting their application.[7,8] Till date, only $BiFeO_3$ based multiferroic materials have shown promising properties with acceptable operational temperatures.[9,10] Hence, there is a need to identify other potential multiferroic materials which can be operational at room temperatures. The κ-Al_2O_3-type family of oxides (e.g. $GaFeO_3$, ε-Fe_2O_3, $AlFeO_3$) are known to possess both ferrimagnetism and ferroelectricity.[11–20] Hence they could be potential alternative for room temperature multiferroic materials, and need to be rigorously studied. The $Ga_xFe_{2-x}O_3$ system was the first compound in this family to be discovered as both ferrimagnetic and magnetoelectric in nature.[21,22] However, unlike $GaFeO_3$, other compounds in this family are metastable phases which cannot be synthesized easily, and hence did not garner much interest. The recent advances in synthesis of nanoparticles and thin films have made stabilization of these phases possible. The ferrimagnetic and ferroelectric properties of these materials could be observed close to room temperature, and are currently being explored for various applications.[11,12,17,18,22–34] The ferrimagnetic nature of materials in this family make it advantageous over $BiFeO_3$, due to better magnetic properties.[35] Orthorhombic $Al_xFe_{2-x}O_3$ (x-AFO) with space group $Pna2_1$, belongs to the same family of oxides. This system is favourable, since it is made up of only 'Al' and 'Fe' cations, both of which are abundantly available, and are non-toxic in nature. Recently, protocols for stabilization of the orthorhombic $AlFeO_3$ phase were established and thin films and nanoparticles were successfully synthesized.[14,36,37] Hence, in the current work, we investigate the ferroelectric and magnetic properties of x-AFO epitaxial thin films deposited by pulsed laser deposition (PLD).

The orthorhombic structure of x-AFO is best described as that consisting of combination of hexagonal and cubic close-packing of oxygen ions. It contains one corner sharing tetrahedral site (Al1), one regular octahedral (Al2) and two heavily distorted octahedral sites (Fe1 and Fe2) which are edge shared (Fig. 1a). Though the cation sites are disordered in nature, the Al1 and Al2 sites are predominantly occupied by Al^{3+} due to their smaller size, while Fe^{3+} prefers the Fe1 and Fe2 sites.[13,35–37] The ferrimagnetism in x-AFO originates from the strong superexchange antiferromagnetic interactions between Fe^{3+} ions,[13] where the Fe^{3+} magnetic moment of Fe1 and Al1 sites are antiparallel to those at Fe2 and Al2 sites. A net magnetic moment in x-AFO mainly arises due to unequal distribution of Fe^{3+} in the four cation sites.[13] In the case of ε-Fe_2O_3, the magnetic moment of Fe^{3+} at

[a] Laboratory for Materials and Structures, Tokyo Institute of Technology, 4259 Nagatsuta, Midori, Yokohama 226-8503, Japan. Email: rao.b.aa@m.titech.ac.jp
[b] Department of Chemistry, The University of Tokyo, Bunkyo-ku, Tokyo 112-0033, Japan
[c] Nanostructures Research Laboratory, Japan Fine Ceramics Center, Atsuta-ku, Nagoya 456-8587, Japan
[d] Center for Materials Research by Information Integration (CMI[2]), Research and Services Division of Materials Data and Integrated System (MaDIS), National Institute for Materials Science (NIMS), 1-2-1 Sengen, Tsukuba, Ibaraki 305-0047, Japan
[e] Department of Applied Physics, National Defence Academy, Yokosuka 239-8686, Japan
Electronic Supplementary Information (ESI) available:

the tetrahedral site (Al1) is smaller compared to the other sites, which gives rise to a net magnetic moment.[11]

While there are some research articles available on polycrystalline $AlFeO_3$ ceramics as well as thin films that have confirmed ferrimagnetism,[36–38] the evidence for piezoelectricity or ferroelectricity have been very scarce.[12,39] Even the ferroelectricity in similar systems like $GaFeO_3$ and ε-Fe_2O_3 is puzzling, since the experimentally observed polarization values were considerably less than that predicted by *ab initio* calculations.[16,40] Recently, Hamasaki *et al.* successfully synthesized epitaxial thin films of *x*-AFO on $SrTiO_3$(111) substrates.[14] However, high leakage currents in the films made direct ferroelectric measurements difficult, and only local information using piezoresponse force microscopy (PFM) could be obtained.[14] Due to this problem, very limited work on the ferroelectric measurements of *x*-AFO is available, thereby making such a study very interesting. The low resistance in thin films is generally due to high density of defects like oxygen-ion vacancies. These can be minimized either by tuning the deposition conditions or by suitable cation doping.[17,41–43] In the present work, we successfully optimized the deposition conditions to obtain *x*-AFO ($0.5 \leq x \leq 1$) films with low leakage current, thereby enabling ferroelectric measurements. While first-principle calculations aided in understanding the mechanism of ferroelectric switching, the discrepancy in the polarization values obtained from theory and experiments is attributed to constraints posed by domains and a dominant contribution from interface effects.

Experimental

Optimization of thin film deposition

x-AFO ($0.5 \leq x \leq 1$) films were deposited on STO(111) single crystal substrates by pulsed laser deposition (PLD) using fourth-harmonic wave of a Nd:YAG laser (λ = 266 nm) with repetition rate of 5 Hz. The films were also deposited on 0.5 wt% Nb-doped STO (111) (Nb:STO) conducting substrates for ferroelectric and magnetocapacitance measurements. As a PLD target, we used *x*-AFO ceramic pellets prepared by solid state synthesis (sintered at 1450°C for 14 hours). Several *x*-AFO films were deposited, and ideal conditions were identified by systematic variation of different parameters such as laser fluence (1 – 4 J/cm^2), oxygen partial pressure (10 mTorr – 500 mTorr), substrate temperature (650°C – 750°C) and annealing method. Single phase films were obtained in all the tested conditions, indicating a wide range of phase stability for the system. It was found that the deposition temperature is the critical parameter to obtain smooth films (fig. S1), while oxygen pressure (P_{O2}) during deposition and annealing is important for obtaining single phase and controlling oxygen vacancies. A low deposition rate is favourable to obtain films with good electrical properties, which is controlled by laser fluence, P_{O2} and target-substrate distance. At higher laser fluence, it was noted that large number of droplets ejected from the target along with the plume, which then deposited on the film as amorphous macro particles, leading to poor quality films (fig. S2). Also, increasing Al content in the target led to increase in the droplet formation on the films (fig. S2). A laser fluence of 1.6 J/cm^2 was found to be suitable for deposition of films of all compositions. The chamber pressure is an important parameter to control the shape of the plume, which improves the uniformity and smoothness of the film. An oxygen atmosphere helps to maintain the stoichiometry of the oxides by reducing oxygen vacancies in the film. P_{O2} of 100 – 300 mTorr was found to be ideal to obtain good quality films with good deposition rate. The substrate temperature controls the grain size and roughness of the films,[44] and a substrate temperature of about 710°C was found to be ideal for the film deposition (fig. S1). Annealing under high P_{O2} can decrease oxygen related defects in the film, which can in turn improve the resistivity of the films (fig. S3). However, optimum annealing temperature is important, since higher annealing temperature can lead to grain growth and increase in surface roughness. We have carried out annealing soon after deposition, in the PLD chamber, with P_{O2} of 100 Torr at 600°C for 30 minutes. After careful consideration, the following PLD conditions were used to deposit the films for further characterization: laser fluence of 1.6 J/cm^2, P_{O2} of 100 mTorr during deposition, substrate temperature of 710°C, and subsequent annealing with P_{O2} of 100 Torr at 600°C for 30 minutes in the PLD chamber. The film thickness was calculated from the Laue fringes observed in the 004 reflection of *x*-ray diffraction, and was found to be 20 – 40 nm for all the compositions studied.

Thin film characterization

The crystal structure of the films was analysed by high-resolution *x*-ray diffraction of Rigaku Smartlab using Cu-Kα_1 radiation. The composition of 0.5-AFO and 1-AFO films were tested using wavelength-dispersive *x*-ray spectroscopy (PW2404 PANalitycal). The actual compositions for the two were found to be x = 0.61 and 1.04 respectively. However, for convenience, the films will be represented based on their target compositions itself. The in-plane magnetizations of the films were measured using a superconducting quantum interference device (SQUID) magnetometer (Quantum Design Co. MPMS XL). The ferroelectric measurements were carried out using the Precision Multiferroic II tester (Radiant Inc.). Out of plane piezoresponse force microscopy measurements were carried out using a frequency tracking DART mode of MFP-3D Asylum Research microscope. The magnetocapacitance measurements were carried out using an LCR meter (Agilent, 4284A), while the samples were loaded inside a Physical Property Measurement System (PPMS, Quantum Design Inc.). For all electric measurements, Pt-top electrode (100 μm diameter) was deposited on the films by electron beam evaporation. While top-top electrode configuration was used for ferroelectric measurements so that symmetrical loops are obtained,[45] other electrical measurements used Pt as top electrode and the Nb:STO substrate as the bottom electrode. X-ray photoelectron spectroscopy (XPS) measurements were carried out on the films using a Versaprobe spectrometer (ULVAC-PHI).

First principles calculation method

The *Ab initio* calculations were performed by the projector-augmented wave (PAW) method within the GGA+U formalism[46] and the framework of density functional theory (DFT),[47,48] as implemented in the VASP code.[49,50] The exchange-correlation interactions were treated by the generalized gradient approximation (GGA-PBE).[51] The on-site Coulomb repulsion was treated at the GGA+*U* level.[52] We adopted the Hubbard effective U_{eff} = 4.0 eV only

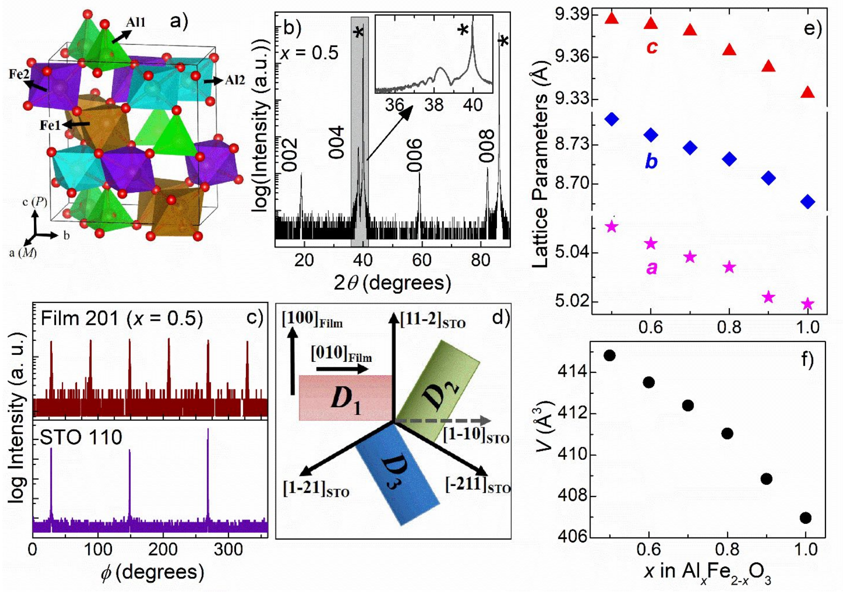

Fig. 1 (a) Crystal structure model of orthorhombic *x*-AFO with space group *Pna*2_1. Al1 indicates the tetrahedral cation site (green), whereas Al2 (blue), Fe1(brown) and Fe2(purple) indicate the octahedral cation site. *P* and *M* indicate the direction of ferroelectric polarization and magnetization respectively. (b) out-of-plane XRD pattern of 0.5-AFO film (* indicates substrate peaks). Inset shows the expanded view of 004 peak. (c) φ scan of 0.5-AFO film deposited on the STO (111) substrate. (d) schematic of orientation relationship between film domains and the substrate. (e) Variation of lattice parameters as a function of *x*. (f) Unit cell volume as a function of *x*.

for the Fe-3*d* electrons. For the PAW potentials, the electronic configurations $3d^{10}4s^2$ for Fe, $3s^23p^1$ for Al and $2s^22p^6$ for O were explicitly treated as valence electrons. The plane wave expansion up to 600 eV was adapted. A *k*-point mesh of 4×2×2 within the 40-atom unit cell was used for Brillouin zone sampling of primitive cells, which was based on the Monkhorst-Pack scheme.[53] The lattice constants and internal atomic coordinates were considered fully optimized once the residual Hellmann-Feynman (HF) forces were less than 1.0×10^{-2} eV/Å. The activation energy for this switching was determined using the nudged elastic band (NEB) method.[54] The polarization values were determined by Berry's phase[55] method implemented in the ABINIT code.[56]

Results

Structural characterization

Figure 1(b) shows the out-of-plane 2θ-θ XRD scan of 0.5-AFO film grown on STO (111) substrates, which shows that a single phase is successfully obtained. Since only 00*l* peaks of the film are observed, it is clear that the film growth is *c*-axis-oriented. The thickness fringes observed in the 004 peak (inset of Fig. 1(b)) indicate smooth film, and was observed for all the compositions studied (Fig. S4-a). The surface topography of the films was also studied using AFM, which showed the RMS roughness of the films to be around 0.6-1.1 nm for all the compositions (Fig. S4-(b-g)). The in-plane crystal-domain orientations of the films were evaluated using φ-scan about the *x*-AFO{201} and STO{110} diffraction peaks (Fig. 1(c)). The films showed six-fold in-plane symmetry of the {201} peak, indicating three types of in-plane domains, where each $[100]_{Film}$ direction is parallel to the $[11\text{-}2]_{STO}$, $[1\text{-}21]_{STO}$, or $[\text{-}211]_{STO}$ direction, as illustrated in figure 1(d). These results are consistent with previous reports of AFO and $GaFeO_3$ based films on STO(111) substrates.[14,57] Figure 1(e) shows the variation of the lattice parameters obtained from in-plane and out-of-plane *x*-ray diffraction, as a function of composition. A decrease in unit cell volume is observed with increasing Al-content (Fig. 1(f)), which is consistent with Vegard's law, as the ionic radii of Al^{3+} is smaller than Fe^{3+}.

Magnetic properties

Figure 2 shows the magnetic properties of *x*-AFO films after subtracting the diamagnetic component of the substrate. Figure 2(a) shows the field cooled temperature dependence of magnetization (*MT*) for different compositions, indicating that the Curie temperature for all the films is above 400 K. Since the maximum operational temperature of the SQUID was 400 K, the exact Curie temperature could not be determined. However, the magnetic measurements on films grown at 300 mTorr oxygen pressure showed relatively lower Curie temperatures (Fig. S5), indicating that Curie point can be tuned by varying oxygen pressure. From figure S1, it is also clear that the Curie temperature decreases with increasing *x*, similar to other reports.[18,37] Figure 2b shows the room temperature magnetization vs. magnetic field hysteresis (*MH*) plots for *x* = 0.5, 0.8 and 0.9, revealing their ferrimagnetic nature. The inset in figure 2b shows the zoomed plot of the *MH* curve, indicating higher coercive field for lower value of *x*.

Figure 2c shows the actual variation of the magnetic coercive field and the saturation magnetization as a function of composition. While the coercive field continuously decreased with increasing *x*, the saturation magnetization was maximum at 0.8-AFO. Pure ε-Fe_2O_3 (*x* = 0), has a very high coercive field due to the strong hybridization of Fe $3d^5$ at the Fe2 site with O 2*p* orbital, resulting from large spin-orbit interaction.[58] The decrease in coercive field with increasing *x*

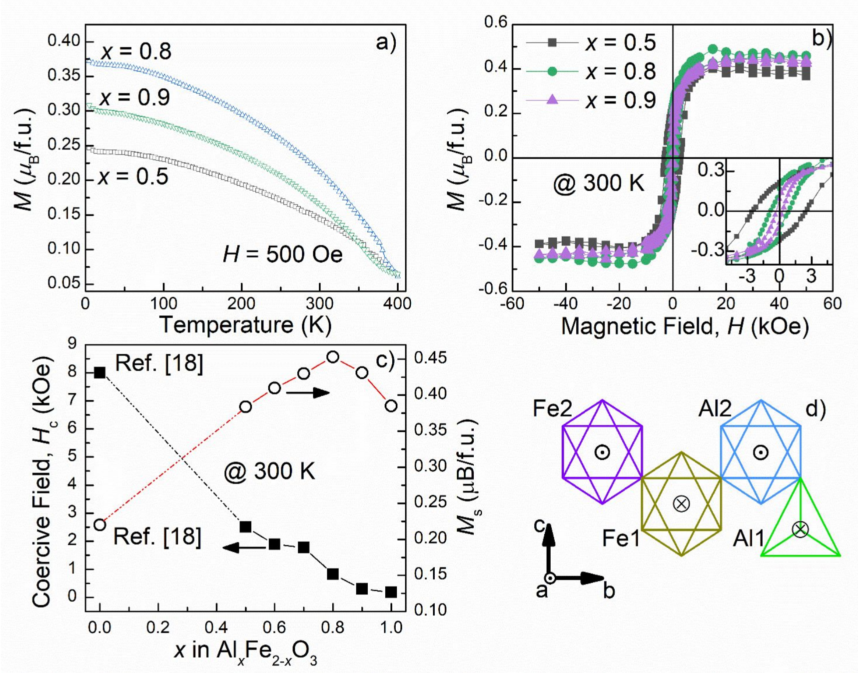

Fig. 2 (a) Field cooled magnetization vs temperature plot for various compositions (*MT*), measured with a constant magnetic field of 500 Oe. (b) Room temperature magnetization vs magnetic field (*MH*) for different compositions, inset shows the zoomed version of the same plot to highlight the differences in the coercive field. (c) Compositional variation of saturation magnetization (M_s) and coercive field (H_c), at room temperature. The values for $x = 0$ have been borrowed from Katayama *et al.*[18] (d) Schematic of the direction of magnetic moments of Fe^{3+} ions at each site. The Fe_2, Al_2 and Fe_1 sites correspond to the octahedral oxygen coordination, whereas the Al1 site corresponds to the tetrahedral coordination. The circles with dot (⊙) indicate the Fe^{3+} spin orientation out of the plane of the paper, while the circles with cross (⊗) indicate spin oriented into the plane of the paper.

(decreasing Fe concentration) must be due to weakening of this phenomenon, since the system is moving away from ε-Fe_2O_3. The reason for maxima in saturation magnetization at $x = 0.8$ can be attributed to the differential occupation of Al^{3+} in each of the four cation sites. This can be explained using figure 2d, which shows an illustration of the magnetic moments of the four cation sites. When $x = 0$ (pure ε-Fe_2O_3), all the sites are completely occupied by Fe^{3+} ions. In this situation, sites Fe1 and Al1 have their spins aligned in one direction and sites Fe2 and Al2 have the spins aligned in the opposite direction. The smaller magnetic moment in the tetrahedral Al1 site results in a net magnetic moment. As *x* increases, for lower values of *x* ($x < 0.8$), the Al^{3+} preferentially occupy the Al1 sites. Since Al1 and Fe1 sites are antiparallel to Al2 and Fe2 sites, the net magnetic moment is given by the algebraic sum of moments from all the sites: $M_{Al2} + M_{Fe2} - M_{Al1} - M_{Fe1}$. Hence, with increasing *x*, the magnetic moment contribution from Al1 site decreases, thereby increasing the net magnetic moment. However, as *x* increases further ($x > 0.8$), Al ions begin to occupy the Al2 sites also, consequently decreasing the net magnetic moment. For films grown at 300 mTorr of oxygen pressure (Fig. S5), it was noted that the magnetic moment of higher composition films ($x \geq 0.8$) had considerably reduced relative to films grown at 100 mTorr. This highlights the significance of oxygen pressure during deposition, on the occupation of Fe^{3+} in the four cation sites.

Ferroelectricity and Magnetocapacitance

While the *x*-AFO system has a non-centrosymmetric structure, it has been difficult to verify its ferroelectricity. The films are prone to leakage, which makes ferroelectric measurements difficult. Though we could observe domain switching as well as butterfly amplitude loop in PFM measurements (Fig. S6), it is difficult to determine the magnitude of polarization by this technique. In addition, non-ferroelectric surfaces are also known to show contrast in PFM measurements under certain conditions.[59–62] Hence, we focussed on direct ferroelectric measurements using a ferroelectric tester, which was possible by obtaining films with improved leakage properties. Figure 3a shows the polarization vs. electric-field (*PE*) hysteresis loops for 1-AFO at different electric fields. All compositions showed similar hysteresis loops (Fig. S7), and domain switching was confirmed by peak in the current vs. electric-field (*IE*) plot, corresponding to the coercive field. However, it was observed that the hysteresis loops from these films do not saturate until the breakdown field, as shown in figure 3a. Figure 3b confirms that both the remnant polarization as well as the coercive field do not saturate with the electric field. This behaviour is different compared to conventional ferroelectrics, which show sudden anomaly in polarization above coercive field, and saturates at higher fields. Absence of sudden jump in remnant polarization of our films indicates that the polarization switching mechanism may be different as compared to conventional ferroelectrics. A continuous increase in the polarization with increasing electric field indicates major contribution from extrinsic effects, which may arise from leakage

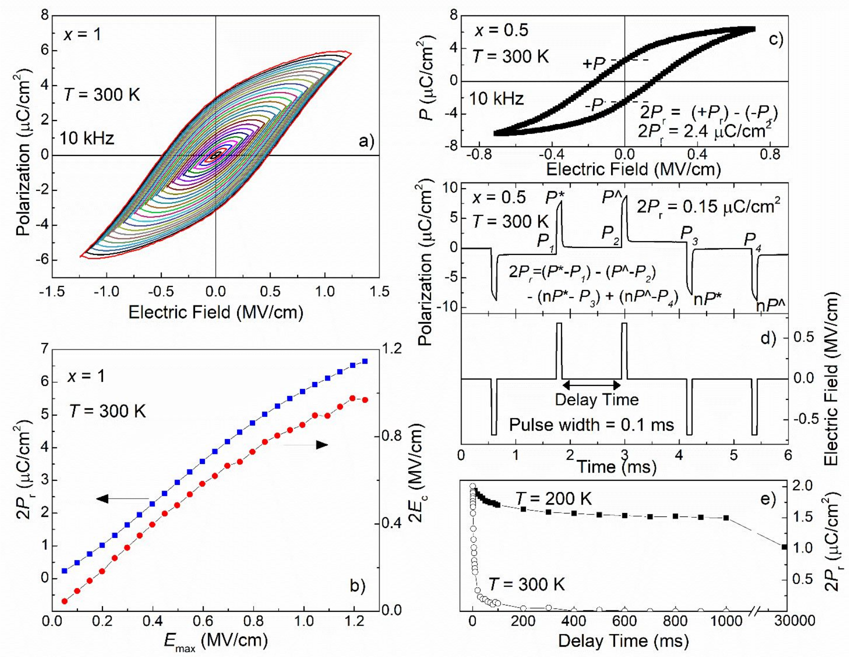

Fig. 3 (a) *PE* hysteresis loops of 1-AFO at 10 kHz, with increasing maximum electric fields. (b) Variation of remnant polarization and coercive field of 1-AFO as a function of maximum electric field, as obtained from (a). (c) Remnant polarization of 0.5-AFO as calculated from *PE* hysteresis. (d) Remnant polarization of 0.5-AFO as calculated from PUND measurement. (e) Remnant polarization of 0.5-AFO film as a function of PUND delay time, measured at 200 K and 300 K.

currents in the film, interface between the film and electrodes, from small domain sizes, etc.[63] However, the peak in *IE* curves indicate polarization switching, which suggests that spontaneous polarization due to ferroelectricity is also present.

To further investigate ferroelectricity in our films, the extrinsic and ferroelectric components of polarization were separated out by the Positive-Up-Negative-Down (PUND) measurement technique.[64] Figure 3c and 3d shows comparison of the remnant polarization

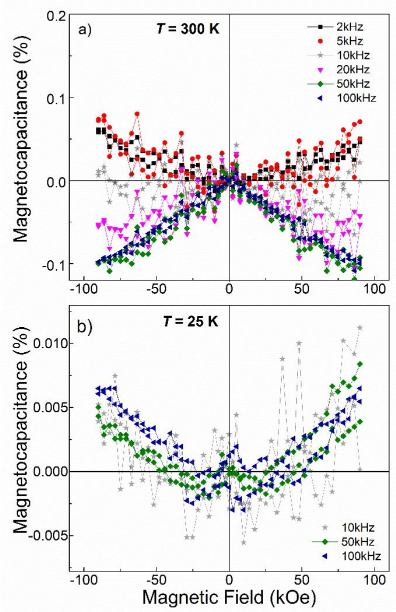

obtained from *PE* hysteresis measurements and PUND measurement for 0.5-AFO film. We can see that the actual remnant polarization obtained from PUND measurement (0.15 μC/cm²) is much smaller than that determined by *PE* loops (2.4 μC/cm²). This is because a large part of the polarization in the film is reversible, which is not completely separated in *PE* measurements. This is also confirmed by observation of large current in the non-switching pulses of PUND measurement (Fig. S8). Similar results were obtained for other compositions of *x*-AFO as well. This proves our earlier proposition that a large component of the polarization at room temperature arises from extrinsic effects. Hence, the PUND measurements are more reliable to extract the remnant polarization in our films. In addition, remnant polarization obtained from PUND measurements showed saturation in polarization upon increasing electric field (Fig. S9), similar to conventional ferroelectrics.

The presence of large extrinsic effects and leakage current leads to a large decrease in the polarization over time at room temperature. In Fig. 3e, as the delay time (delay time is the time gap between the two up (or down) pulses of PUND measurement) in the room temperature PUND measurement is increased, the remnant polarization decreases rapidly. Hence, to confirm intrinsic ferroelectricity, we carried out ferroelectric measurements at lower temperatures where the extrinsic contributions and leakage are considerably small. PUND measurements at 200 K showed persistence of significant remnant polarization even with a delay time of 30 s (Fig. 3e), which strongly indicates presence of intrinsic ferroelectric polarization. However at low temperatures, we could not observe good hysteresis in the *PE* loop measurements, since the coercive field of the films become very large and are often above the breakdown field.

Fig. 4 MC measurements of 0.8-AFO film (a) at 300 K, which shows frequency dependence due to extrinsic contributions. (b) at 25 K, showing the frequency independent intrinsic MC effect of the film.

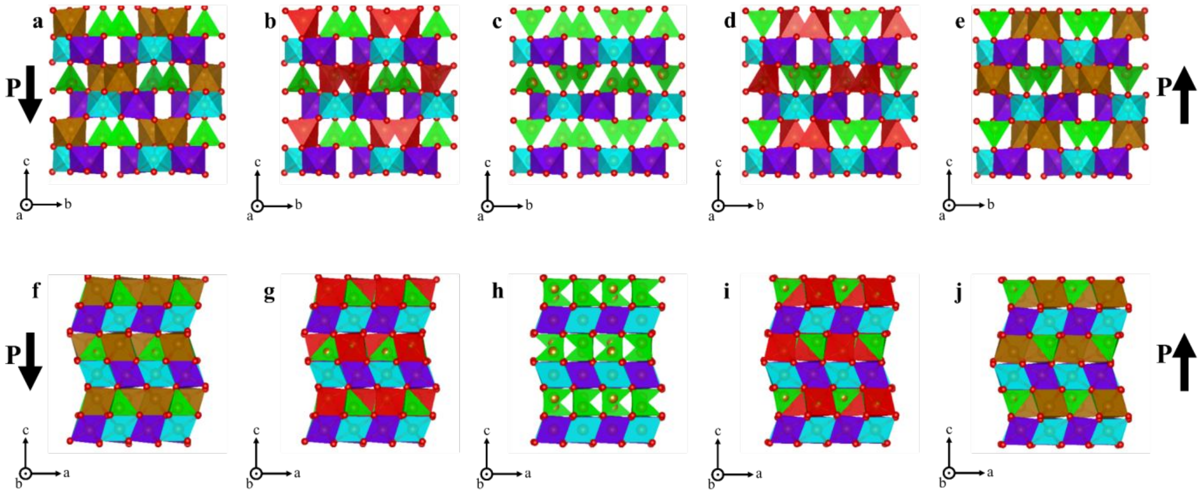

Fig. 5 Illustration of structural changes upon polarization reversal. (a-e) structure viewed along *a*-axis, (f-j) structure viewed along *b*-axis. The 3 octahedral sites are indicated in purple (Fe1), brown (Fe2) and blue (Al1), and the tetrahedral site in green (Al1). The intermediate pentahedra is indicated in red.

Since our films showed both ferroelectricity as well as ferrimagnetism, we also carried out magnetocapacitance (MC) measurements to see if there was any coupling between the two orders. Figure 4 shows the results from MC measurements on the 0.8-AFO film, which showed strong frequency dependence at room temperature. This is probably due to presence of extrinsic contribution in the measurements. In order to separate out the extrinsic effects, we carried out MC measurements at 25 K, which showed a positive MC effect irrespective of the frequency. This confirms the existence of intrinsic MC coupling in the *x*-AFO system.

First-Principles Calculation

Theoretically determined activation energies and polarization switching mechanisms of *x*-AFO are discussed based on *ab initio* calculations performed on κ-Al_2O_3 and ε-Fe_2O_3. One possible mechanism of polarization switching of κ-Al_2O_3 type *x*-AFO is via an intermediate non-polar centrosymmetric state.[16,65] Earlier, Stoeffler *et al*. calculated the activation energy and net polarization of isostructural $GaFeO_3$ by considering a *Pnna* space group as the intermediate state.[16] However, the reported activation energy for the polarization switching was 0.5 eV, which is much larger than that seen in conventional ferroelectric compounds (e.g. $BaTiO_3$ – 0.02 eV[66], $PbTiO_3$ – 0.03 eV[67]). Xu *et al.* suggested an alternative centrosymmetric space group *Pbcn*, which gave a much lower activation energy for polarization in ε-Fe_2O_3.[68] Hence, we considered the *Pbcn* space group as the non-polar polarized structure for our calculation. Figures 5(a-e) show the schematic of transition from a negatively polarized structure to centrosymmetric, and then to a positively polarized structure. The calculation yielded activation energies for polarization switching of 0.088 and 0.155 eV/f.u for ε-Fe_2O_3 and κ-Al_2O_3 respectively (Fig. S10). We can expect the activation energies for the intermediate *x*-AFO structures also to be of similar order. These values are fairly small and acceptable, compared to the high value previously reported for $GaFeO_3$.[16,65] During the polarization reversal process, the polarization switches from $-P_s$ to $+P_s$, while smoothly passing through zero (Fig. 5(e, h). Viewing the structure along the *b*-axis clearly explains the polarization switching mechanism (Fig 5(f-j)). Close-packed oxygen layers in corundum layers keep their octahedral shape during the switching. However, oxygen above and below the corundum layers shift along *a*-axis, in opposite directions relative to each other. This shearing motion of oxygen layers induces a coordination switching of cations Fe1 and Al1 sites. An originally tetrahedral(octahedral) Al1(Al2) site turns into octahedral(tetrahedral) Al2(Al1) site after the polarization switching. This mechanism is quite different from conventional ferroelectric oxides, where cations and anions move in opposite directions in a linear manner (Slater mode).[69]

By using the Berry's phase approach[55], the polarization of Al_2O_3 and ε-Fe_2O_3 was calculated to be about 26 $\mu C/cm^2$ and 21 $\mu C/cm^2$ respectively. Since there is no structure change in the substituted *x*-AFO series, their theoretical polarization values will also lie in between 21 - 26 $\mu C/cm^2$. While this value of polarization is comparable to theoretical values reported for other isostructural compounds like $GaFeO_3$ and ε-Fe_2O_3,[16,40,65,68] it is about two orders of magnitude larger than that observed experimentally. Similar ambiguity is observed in $GaFeO_3$ based films as well, and the exact reason for this is not yet known. We speculate that the multi-domain structure of the thin film obstructs complete polarization reversal, as there is in-plane shearing of oxygen layers involved. Hence the actual polarization is considerably lesser than that predicted.

Discussion

κ-Al_2O_3 type ferrites like ε-Fe_2O_3, $GaFeO_3$ and $AlFeO_3$ have recently been identified to be promising compounds displaying both ferrimagnetism as well as ferroelectricity.[17,18,25,28] Especially, the ferrimagnetic nature of these ferrites, which can be stabilized above room temperature, is very interesting. While the large coercive field and magnetic anisotropy of ε-Fe_2O_3 has already made it interesting for high-frequency millimeter wave absorption,[25] the research on ferroelectric and multiferroic properties of these ferrites is still in its nascent stage. Recently, Katayama *et. al*. showed that the properties of κ-Al_2O_3 type $GaFeO_3$ can be tuned by suitable cation substitution, to obtain excellent ferroelectric and magnetic properties at room temperature.[17] The *x*-AFO system is made of only '*Al*' and '*Fe*' ions, both of which are abundantly available and are non-toxic in nature.

Hence, it can be a potential game changer in the electronic industry, if good ferroelectric and magnetic properties can be established in this system. The magnetic properties are easier to be tuned, and a Curie temperature above room temperature could be established. The Curie temperature can be tuned either by cation substitution or by varying oxygen pressure during deposition. Jaffe *et al.* suggested that *n*-type carriers present due to oxygen vacancy in semiconducting ferromagnets help mediate magnetic interactions between spins.[70] A similar phenomenon may be effecting the *x*-AFO system as well, as a consequence of which the Curie temperature is influenced by oxygen vacancy concentration.[71]

While the magnetic properties of the films could be easily comprehended, their ferroelectric properties are quite complex. In addition, extrinsic contribution adds to the complexity of the ferroelectric measurements. *PE* hysteresis measurements showed remnant polarization values of around 1 – 5 μC/cm^2 and it did not saturate with increasing electric field. However, PUND measurements could successfully separate the extrinsic contribution to a large extent, and it showed the true value of intrinsic polarization to be about one order less. Using results from PUND measurements, saturation of the remnant polarization with increasing electric field was observed, which also advocates the ferroelectric nature of the films. We further confirmed the ferroelectric nature of the films by carrying out PUND measurements at 200 K, which showed the intrinsic polarization to be stable for more than 30 s, typical of a ferroelectric material. Our study also demonstrates the challenges posed by extrinsic effects as well as leakage problems in the ferroelectric measurements of thin films.

Though theoretical predictions state much larger polarization (~21-26 μC/cm^2), the actual value is about two order less. This ambiguity has been observed for other systems in the family ($GaFeO_3$, ε-Fe_2O_3) as well.[16,68] We suggest that the existence of multiple in-plane domains in the film could be the reason behind reduced polarization. As first-principle calculation suggested that the domain switching along *c*-axis (out-of-plane) takes place by shearing of oxygen layers along *a*-axis, presence of multiple in-plane domains can make such a shearing very difficult. The *x*-ray diffraction ϕ-scans of the films in figure 1d clearly show presence of three types of crystal domains, adhering to the 3-fold symmetry of the STO(111) substrate. Any attempt in shearing of oxygen from domain 1 will be constricted by domains 2 and 3, and likewise, shearing in domains 2 and 3 will also be restricted (Fig. 6). Hence, when electric field is applied, the domains can orient only to a small extent, and they tend to go back to the original position upon removal of the electric field. The small remnant polarization observed could be due to existence of oxygen vacancies at the domain walls, which can give a small degree of freedom for the domains to switch. Presence of oxygen vacancies is reasonable, since XPS measurement on our films showed evidence for presence of Fe^{2+} along with Fe^{3+} ions (Fig. S11). These oxygen vacancies generally aggregate near domain boundaries, and since TEM observations have shown the domain size to be very small (5-10 nm)[37], the defect density in the film could be very high. The cation charge deficiency caused due to presence of Fe^{2+} ions is usually balanced by formation of oxygen vacancies.[72]

If we can grow films with single crystal domain, then it is likely that polarization values close to that of theoretical calculations can be obtained. An extensive work on domain engineering is required to obtain single domain films of *x*-AFO. Preliminary work by Katayama *et al.* on $Ga_{0.6}Fe_{1.4}O_3$ films showed that STO(111) yields the minimum number of in-plane domains compared to several other substrates.[57] Also, using STO(100) and STO(110) oriented substrates yielded six in-plane crystal domains, which is double of that obtained in STO(111). Hence, among all the substrates studied so far, STO(111) yields the least number of in-plane domain types. Further research on more substrates and deposition conditions is required to achieve single domain films. One of the possible approach could be to promote single domain growth using vicinal substrates, where some researchers have obtained success.[73]

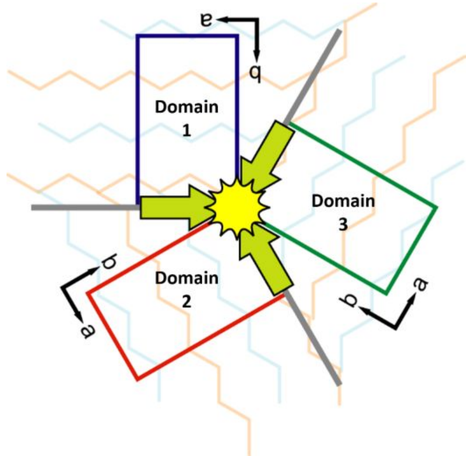

Fig. 6 Illustration of obstruction to polarization switching in the multi-domain structure, which occurs by in-plane shearing of the oxygen layers.

Xu *et al.* have shown by theoretical calculations that cation size is an important factor in stabilizing the ferroelectric phase.[68] A decrease in the cation size stabilizes the ferroelectric phase, and since the radius of Al^{3+} (0.535 Å) is smaller than that of Fe^{3+} (0.55Å and 0.645Å in high and low spin state respectively), increasing *x* should improve the ferroelectric property of the system. However, in the present study, we could not establish any composition dependence of ferroelectric properties. Since the polarization reversal in these systems occurs in an indirect manner, many intricate parameters like oxygen vacancy concentration, occupancy of each cation site, defect population, etc., may supersede the effect due to cation size. Observation of weak magnetocapacitance effect indicates existence of coupling between magnetic and electrical characteristics of the film. However, more studies are required to ascertain the true coupling behaviour.

Conclusions

While room temperature ferrimagnetism could be easily established in the *x*-AFO system, the room temperature ferroelectric measurements were obscured by extrinsic contributions. However, low temperature PUND measurements confirmed existence of intrinsic ferroelectricity in the films. PUND measurements proved to be better at providing reliable remnant polarization values. The low polarization in the films could be attributed to constraints posed by multiple in-plane domains. However, we hope that the current work will motivate fabrication of single domain films, which can probably yield polarization values close to the theoretical ones. The magnetic measurements were consistent with other works, and the Curie temperature and coercive field were found to decrease with increasing *Al* content. Simultaneous presence of both magnetism and ferroelectricity in the *x*-AFO system, along with the evidence of magnetocapacitance, makes this system very interesting as a potential multiferroic material.

Conflicts of interest

There are no conflicts to declare.

Acknowledgements

B.N.R. acknowledges fellowship support by JSPS(P17079). This work was partly supported by JSPS KAKENHI Grants-in-Aid for challenging Research (Pioneering) (M.I., 1706420), (Exploratory) (Sh.Y., 18K19126), Scientific Research (B) (S.Y., 19H02426) and MEXT Elements Strategy Initiative to form Core Research Centre, Collaborative Research Project of Laboratory for Materials and Structures, Institute of Innovative Research, Tokyo Institute of Technology. H.M. acknowledges "Materials research by Information Integration" Initiative (MI2I) project of the Support Program for Starting Up Innovation Hub from Japan Science and Technology Agency (JST).

References

1 W. Eerenstein, N. D. Mathur and J. F. Scott, *Nature*, 2006, **442**, 759–765.
2 R. Ramesh and N. A. Spaldin, *Nat. Mater.*, 2007, **6**, 21–29.
3 J. F. Scott, *Nat. Mater.*, 2007, **6**, 256–257.
4 D. S. Jeong, R. Thomas, R. S. Katiyar, J. F. Scott, H. Kohlstedt, A. Petraru and C. S. Hwang, *Rep. Prog. Phys.*, 2012, **75**, 076502.
5 T. Nan and N. X. Sun, in *Composite Magnetoelectrics*, eds. G. Srinivasan, S. Priya and N. X. Sun, Woodhead Publishing, 2015, pp. 329–356.
6 M. Fiebig, T. Lottermoser, D. Meier and M. Trassin, *Nat. Rev. Mater.*, 2016, **1**, 16046.
7 S. Dong, J.-M. Liu, S.-W. Cheong and Z. Ren, *Adv. Phys.*, 2015, **64**, 519–626.
8 J. F. Scott, *NPG Asia Mater.*, 2013, **5**, e72.
9 J. Wang, J. B. Neaton, H. Zheng, V. Nagarajan, S. B. Ogale, B. Liu, D. Viehland, V. Vaithyanathan, D. G. Schlom, U. V. Waghmare, N. A. Spaldin, K. M. Rabe, M. Wuttig and R. Ramesh, *Science*, 2003, **299**, 1719–1722.
10 W. Eerenstein, F. D. Morrison, J. Dho, M. G. Blamire, J. F. Scott and N. D. Mathur, *Science*, 2005, **307**, 1203–1203.
11 M. Gich, C. Frontera, A. Roig, E. Taboada, E. Molins, H. R. Rechenberg, J. D. Ardisson, W. A. A. Macedo, C. Ritter, V. Hardy, J. Sort, V. Skumryev and J. Nogués, *Chem. Mater.*, 2006, **18**, 3889–3897.
12 G. M. Santos, D. M. Silva, V. F. Freitas, G. S. Dias, A. A. Coelho, M. Pal, I. A. Santos, L. F. Cótica, R. Guo and A. S. Bhalla, *Ferroelectrics*, 2014, **460**, 108–116.
13 F. Bouree, J. L. Baudour, E. Elbadraoui, J. Musso, C. Laurent and A. Rousset, *Acta Crystallogr. B*, 1996, **52**, 217–222.
14 Y. Hamasaki, T. Shimizu, H. Taniguchi, T. Taniyama, S. Yasui and M. Itoh, *Appl. Phys. Lett.*, 2014, **104**, 082906.
15 R. Saha, A. Shireen, S. N. Shirodkar, U. V. Waghmare, A. Sundaresan and C. N. R. Rao, *Solid State Commun.*, 2012, **152**, 1964–1968.
16 D. Stoeffler, *J. Phys. Condens. Matter*, 2012, **24**, 185502.
17 T. Katayama, S. Yasui, Y. Hamasaki, T. Osakabe and M. Itoh, *J. Mater. Chem. C*, 2017, **5**, 12597–12601.
18 T. Katayama, S. Yasui, Y. Hamasaki, T. Shiraishi, A. Akama, T. Kiguchi and M. Itoh, *Adv. Funct. Mater.*, 2018, **28**, 1704789.
19 M. Trassin, N. Viart, G. Versini, J.-L. Loison, J.-P. Vola, G. Schmerber, O. Crégut, S. Barre, G. Pourroy, J. H. Lee, W. Jo and C. Mény, *Appl. Phys. Lett.*, 2007, **91**, 202504.
20 Z. H. Sun, Y. L. Zhou, S. Y. Dai, L. Z. Cao and Z. H. Chen, *Appl. Phys. A*, 2008, **91**, 97–100.
21 J. P. Remeika, *J. Appl. Phys.*, 1960, **31**, S263–S264.
22 G. T. Rado, *Phys. Rev. Lett.*, 1964, **13**, 335–337.
23 J. Jin, S. Ohkoshi and K. Hashimoto, *Adv. Mater.*, 2004, **16**, 48–51.
24 R. Saha, A. Shireen, S. N. Shirodkar, U. V. Waghmare, A. Sundaresan and C. N. R. Rao, *J. Solid State Chem.*, 2011, **184**, 2353–2359.
25 A. Namai, M. Yoshikiyo, K. Yamada, S. Sakurai, T. Goto, T. Yoshida, T. Miyazaki, M. Nakajima, T. Suemoto, H. Tokoro and S. Ohkoshi, *Nat. Commun.*, 2012, **3**, 1035.
26 A. Thomasson, S. Cherifi, C. Lefevre, F. Roulland, B. Gautier, D. Albertini, C. Meny and N. Viart, *J. Appl. Phys.*, 2013, **113**, 214101.
27 S. Mukherjee, A. Roy, S. Auluck, R. Prasad, R. Gupta and A. Garg, *Phys. Rev. Lett.*, 2013, **111**, 087601.
28 M. Gich, I. Fina, A. Morelli, F. Sánchez, M. Alexe, J. Gàzquez, J. Fontcuberta and A. Roig, *Adv. Mater.*, 2014, **26**, 4645–4652.
29 S. Ohkoshi, A. Namai, M. Yoshikiyo, K. Imoto, K. Tamazaki, K. Matsuno, O. Inoue, T. Ide, K. Masada, M. Goto, T. Goto, T. Yoshida and T. Miyazaki, *Angew. Chem. Int. Ed.*, 2016, **55**, 11403–11406.
30 S. Ohkoshi, K. Imoto, A. Namai, S. Anan, M. Yoshikiyo and H. Tokoro, *J. Am. Chem. Soc.*, 2017, **139**, 13268–13271.
31 K. Knížek, M. Pashchenko, P. Levinský, O. Kaman, J. Houdková, P. Jiříček, J. Hejtmánek, M. Soroka and J. Buršík, *J. Appl. Phys.*, 2018, **124**, 213904.
32 T. Katayama, S. Yasui, T. Osakabe, Y. Hamasaki and M. Itoh, *Chem. Mater.*, 2018, **30**, 1436–1441.
33 T. Katayama, T. Osakabe, S. Yasui, Y. Hamasaki, B. N. Rao, M. Zhang and M. Itoh, *Appl. Phys. Lett.*, 2018, **113**, 162901.
34 Y. Hamasaki, T. Shimizu, S. Yasui, T. Taniyama and M. Itoh, *Appl. Phys. Lett.*, 2016, **109**, 162901.
35 S. Ohkoshi, A. Namai and S. Sakurai, *J. Phys. Chem. C*, 2009, **113**, 11235–11238.
36 R. Saha, A. Shireen, A. K. Bera, S. N. Shirodkar, Y. Sundarayya, N. Kalarikkal, S. M. Yusuf, U. V. Waghmare, A. Sundaresan and C. N. R. Rao, *J. Solid State Chem.*, 2011, **184**, 494–501.
37 Y. Hamasaki, T. Shimizu, S. Yasui, T. Shiraishi, A. Akama, T. Kiguchi, T. Taniyama and M. Itoh, *J. Appl. Phys.*, 2017, **122**, 015301.
38 L. F. Cótica, G. M. Santos, V. F. Freitas, A. A. Coelho, M. Pal, I. A. Santos, D. Garcia, J. A. Eiras, R. Guo and A. S. Bhalla, *J. Appl. Phys.*, 2015, **117**, 064104.
39 P. Kumar, A. Bera, D. V. S. Muthu, S. N. Shirodkar, R. Saha, A. Shireen, A. Sundaresan, U. V. Waghmare, A. K. Sood and C. N. R. Rao, *Phys. Rev. B*, 2012, **85**, 134449.
40 G. M. Santos, I. B. Catellani, I. A. Santos, R. Guo, A. S. Bhalla, J. E. Padilha and L. F. Cótica, *Sci. Rep.*, 2018, **8**, 6420.

41 M. F. Zhang, Y. Wang, K. F. Wang, J. S. Zhu and J.-M. Liu, *J. Appl. Phys.*, 2009, **105**, 061639.
42 W. Zhang, L. Li and X. M. Chen, *J. Appl. Phys.*, 2009, **106**, 104108.
43 L. Yao, S. Inkinen and S. van Dijken, *Nat. Commun.*, 2017, **8**, 14544.
44 W. Zhang, S. Wu and X. Chen, *Chin. Sci. Bull.*, 2013, **58**, 3398–3402.
45 F. Liu, I. Fina, R. Bertacco and J. Fontcuberta, *Sci. Rep.*, 2016, **6**, 25028.
46 P. E. Blöchl, *Phys. Rev. B*, 1994, **50**, 17953–17979.
47 P. Hohenberg and W. Kohn, *Phys. Rev.*, 1964, **136**, B864–B871.
48 W. Kohn and L. J. Sham, *Phys. Rev.*, 1965, **140**, A1133–A1138.
49 G. Kresse and J. Furthmüller, *Phys. Rev. B*, 1996, **54**, 11169–11186.
50 G. Kresse and D. Joubert, *Phys. Rev. B*, 1999, **59**, 1758–1775.
51 J. P. Perdew, K. Burke and M. Ernzerhof, *Phys. Rev. Lett.*, 1996, **77**, 3865–3868.
52 S. L. Dudarev, G. A. Botton, S. Y. Savrasov, C. J. Humphreys and A. P. Sutton, *Phys. Rev. B*, 1998, **57**, 1505–1509.
53 H. J. Monkhorst and J. D. Pack, *Phys. Rev. B*, 1976, **13**, 5188–5192.
54 G. Mills, H. Jónsson and G. K. Schenter, *Surf. Sci.*, 1995, **324**, 305–337.
55 R. D. King-Smith and D. Vanderbilt, *Phys. Rev. B*, 1993, **47**, 1651–1654.
56 X. Gonze, J.-M. Beuken, R. Caracas, F. Detraux, M. Fuchs, G.-M. Rignanese, L. Sindic, M. Verstraete, G. Zerah, F. Jollet, M. Torrent, A. Roy, M. Mikami, Ph. Ghosez, J.-Y. Raty and D. C. Allan, *Comput. Mater. Sci.*, 2002, **25**, 478–492.
57 T. Katayama, S. Yasui, Y. Hamasaki and M. Itoh, *Appl. Phys. Lett.*, 2017, **110**, 212905.
58 M. Yoshikiyo, K. Yamada, A. Namai and S. Ohkoshi, *J. Phys. Chem. C*, 2012, **116**, 8688–8691.
59 A. S. Borowiak, N. Baboux, D. Albertini, B. Vilquin, G. Saint Girons, S. Pelloquin and B. Gautier, *Appl. Phys. Lett.*, 2014, **105**, 012906.
60 N. Balke, P. Maksymovych, S. Jesse, A. Herklotz, A. Tselev, C.-B. Eom, I. I. Kravchenko, P. Yu and S. V. Kalinin, *ACS Nano*, 2015, **9**, 6484–6492.
61 M. Andrä, F. Gunkel, C. Bäumer, C. Xu, R. Dittmann and R. Waser, *Nanoscale*, 2015, **7**, 14351–14357.
62 H. Miao, C. Tan, X. Zhou, X. Wei and F. Li, *EPL Europhys. Lett.*, 2014, **108**, 27010.
63 S. Trolier-Mckinstry, J. F. S. Jr, J. L. Lacey, T. Su, G. Zavala and J. Fendler, *Ferroelectrics*, 1998, **206**, 381–392.
64 H. Naganuma, Y. Inoue and S. Okamura, *Appl. Phys. Express*, 2008, **1**, 061601.
65 S. Song, H. M. Jang, N.-S. Lee, J. Y. Son, R. Gupta, A. Garg, J. Ratanapreechachai and J. F. Scott, *NPG Asia Mater.*, 2016, **8**, e242.
66 R. E. Cohen and H. Krakauer, *Phys. Rev. B*, 1990, **42**, 6416–6423.
67 U. V. Waghmare and K. M. Rabe, *Phys. Rev. B*, 1997, **55**, 6161–6173.
68 K. Xu, J. S. Feng, Z. P. Liu and H. J. Xiang, *Phys. Rev. Appl.*, 2018, **9**, 044011.
69 J. C. Slater, *Phys. Rev.*, 1950, **78**, 748–761.
70 J. E. Jaffe, T. C. Droubay and S. A. Chambers, *J. Appl. Phys.*, 2005, **97**, 073908.
71 B. N. A. Rao, S. Yasui, T. Katayama and M. Itoh, *MRS Adv.*, 2019, **4**, 539–544.
72 V. G. Bhide and H. C. Bhasin, *Phys. Rev.*, 1968, **172**, 290–294.
73 C. Ma, M. Liu, C. Chen, Y. Lin, Y. Li, J. S. Horwitz, J. Jiang, E. I. Meletis and Q. Zhang, *Sci. Rep.*, 2013, **3**, 3092.

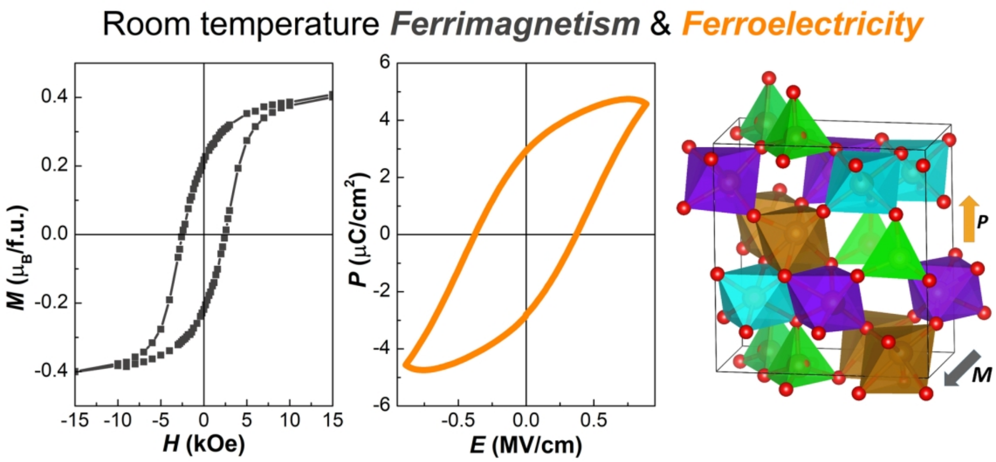

80x36mm (600 x 600 DPI)